ISSN:2731-538X | E-ISSN:2731-5398
Vol. 20 No. 01 (2026)

INVESTIGATION OF A CLOSED-LOOP CONTROLLED PERFORMANCE OF POTASSIUM-ION BATTERIES WITH PHOTO VOLTAIC OPERATED ELECTRIC VEHICLE.

M.Gnanaprakash[a], S.P.Mangaiyarkarasi[a], D.Periyaazhagar[b]. M.Suman[c]
[a]Department of Electrical and Electronics Engineering, University College of Engineering, Panruti. Tamilnadu, India. 607106.
[b] Department of Electrical and Electronics Engineering, Krishnasamy College of Engineering and Technology, Cuddalore, Tamil Nadu, India. 607109.
[c] Department of Electrical and Electronics Engineering, Mahabarathi Engineering College, Kallakurichi,Tamil Nadu, India 606201.

ABSTARCT:
The global transition toward clean transportation has accelerated the demand for advanced, sustainable, and high-performance energy storage systems for electric vehicles. Lithium-ion batteries (LIBs), despite their market dominance, face pressing challenges such as rising costs, resource scarcity, and safety concerns, prompting the search for viable alternatives. Potassium-ion batteries (KIBs) have emerged as promising candidates due to potassium's abundance, low cost, and electrochemical potential comparable to lithium. In particular, $K_3V_2(PO_4)_3/C$ nanocomposites exhibit superior ionic conductivity, three-dimensional diffusion channels, and enhanced cycling stability, making them suitable for next-generation EV applications. This paper focuses on the synthesis, characterization, and system-level integration of $K_3V_2(PO_4)_3/C$ nanocomposites as advanced cathode materials. Beyond energy storage, these composites demonstrated multifunctionality through efficient photocatalytic degradation of organic dyes and strong antioxidant properties, broadening their scope into environmental and biomedical applications. Six control strategies—Proportional–Integral (PI), Fractional-Order PID (FOPID), Sliding Mode Control (SMC), Model Predictive Control (MPC), Hysteresis Control (HC), and Fuzzy Logic Control (FLC)—were comparatively analyzed for their effectiveness in managing energy flow, mitigating battery stress, and enhancing system efficiency.
The results demonstrate that the proposed system significantly improves vehicle performance by reducing battery degradation, ensuring efficient regenerative braking, and maintaining stable operation across diverse drive cycles. Among the controllers, intelligent and predictive strategies such as FLC and MPC offered superior adaptability to nonlinearities, uncertainties, and fluctuating power demands, while conventional methods provided simplicity and ease of implementation. The contributions underscore the feasibility of KIB-based ESS with renewable integration as a pathway to next-generation, sustainable, and high-efficiency electric vehicles.
Keywords: Potassium-ion batteries; electric vehicles; Bidirectional buck–boost converter; Energy management system; Model predictive control; Fuzzy logic control; Sliding Mode Control ; Hysteresis Control .

1. Introduction
The rapid growth of global energy demand, driven by industrial development and transportation needs, has intensified concerns regarding greenhouse gas (GHG) emissions, fossil fuel dependency, and climate change. The transportation sector alone accounts for nearly one-quarter of global GHG emissions, primarily from internal combustion engine (ICE) vehicles [1]. To

ISSN:2731-538X | E-ISSN:2731-5398
Vol. 20 No. 01 (2026)

address these environmental and energy security challenges, electrification of transportation through electric vehicles (EVs) and hybrid electric vehicles (HEVs) has gained significant attention worldwide.

Energy storage systems (ESS) are the backbone of EV and HEV powertrains, as their performance directly determines driving range, fuel economy, and system reliability. Lithium-ion batteries (LIBs) dominate current applications due to their high energy density, efficiency, and established manufacturing base [2,3]. However, several limitations hinder their long-term sustainability, including rising costs, safety concerns such as thermal runaway, and dependence on geographically concentrated lithium and cobalt reserves [4–6]. These issues highlight the urgent need for alternative battery chemistries that are more sustainable, safer, and cost-effective.

Potassium-ion batteries (KIBs) have recently emerged as promising candidates for large-scale applications due to the natural abundance of potassium, low material costs, and comparable redox potential (−2.93 V vs. SHE) to lithium (−3.04 V vs. SHE) [7–9]. Unlike sodium, potassium can intercalate efficiently into graphite, enabling the use of mature electrode technologies [10]. Among various cathode options, NASICON-type $K_3V_2(PO_4)_3$ (KVP) and its carbon composites (KVP/C) have demonstrated stable cycling, high operating voltage (~3.6–3.9 V), and improved electronic conductivity [11–13]. These characteristics make KIBs particularly attractive for EVs, where both high energy and power densities are essential.

Beyond material-level advancements, system-level integration of KIBs into renewable inputs like photovoltaic (PV) modules—managed by power electronic converters and an energy management system (EMS). The EMS plays a critical role in balancing power flows, minimizing battery degradation, and ensuring stable performance under varying load and driving conditions [14,15]. While extensive research has focused on LIB-based ESS, limited work has investigated KIB integration, especially in PV-powered EVs.

Control strategies are equally important for efficient ESS operation. Conventional controllers such as Proportional–Integral (PI) are simple but often inadequate for nonlinear and dynamic EV environments. Advanced methods including Fractional-Order PID (FOPID), Sliding Mode Control (SMC), Model Predictive Control (MPC), Hysteresis Control (HC), and Fuzzy Logic Control (FLC) offer improved robustness, predictive optimization, or adaptability to uncertainties [16–20]. However, comprehensive comparisons of these controllers in renewable-assisted, KIB-based EVs are scarce.

This work addresses these research gaps by developing and evaluating a PV-assisted HESS incorporating $K_3V_2(PO_4)_3$/C-based KIBs, ultracapacitors, and bidirectional buck–boost converters. Six control strategies (PI, FOPID, SMC, MPC, HC, and FLC) are implemented and compared under both simulation and experimental conditions. The contributions of this paper are summarized as follows:

Development of an energy storage system integrating PV and KIBs for EV applications. Modelling and simulation of six control strategies for DC bus regulation, battery management, and motor speed control. Comparative analysis highlighting the strengths and limitations of each control approach, with emphasis on MPC and FLC as the most effective for dynamic EV operation.

2. Literature Review

2.1 Potassium-ion batteries and cathode materials

ISSN:2731-538X | E-ISSN:2731-5398
Vol. 20 No. 01 (2026)

LIBs dominate current markets owing to their maturity, yet issues of cost, safety, and resource scarcity hinder scalability [2–6]. Potassium-ion batteries (KIBs) are gaining attention because potassium is abundant, low-cost, and exhibits an electrochemical potential comparable to lithium [7–9]. Furthermore, unlike sodium, potassium intercalates into graphite anodes, enabling compatibility with existing electrode technologies [10].

Among cathodes, NASICON-type $K_3V_2(PO_4)_3$ (KVP) is particularly attractive, offering high operating voltages and stable cycling. However, its low electronic conductivity is a drawback. This limitation has been overcome by synthesizing KVP/C composites, which achieve high capacity, fast kinetics, and long cycle life [11–13]. These properties align well with the requirements of EVs, which demand both high energy and high power density.

2.2 Electric Vehicles and Energy Management

EVs combine batteries and PV panels to improve efficiency and reliability. The energy management system (EMS) is responsible for power sharing and optimal operation. Conventional rule-based approaches are easy to implement but often suboptimal under real-world conditions [14]. Advanced EMS with renewable integration has demonstrated improved efficiency, but fluctuating solar input requires robust control strategies to ensure stable operation [15].

2.3 Control strategies for EV converters

Control of power electronic converters is central to effective EMS operation. PI controllers are simple and widely used but are weak under nonlinear dynamics [16]. FOPID introduces fractional-order terms, enhancing flexibility and robustness [16]. SMC offers robustness against disturbances but suffers from chattering [17]. MPC provides predictive optimization with explicit constraint handling, making it highly effective but computationally demanding [18]. HC delivers fast response but variable switching frequency reduces efficiency. FLC provides model-free adaptability to nonlinearities and uncertainties, though its performance depends on well-designed rule sets [19,20].

2.4 Research gap

While LIB-based EV control has been extensively studied, very limited work has addressed KIB integration in renewable-assisted systems. Moreover, comparative analyses of classical, nonlinear, predictive, and intelligent controllers in such architectures are lacking. This study addresses these gaps through simulation and experimental evaluation of six controllers in a PV–KIB ESS.

3. Modeling and Investigation of a Closed-Loop Controlled Multi-Converter System PV Arrays powered Potassium-Ion Batteries in Electric Vehicles

The rapid evolution of transportation technology, coupled with rising concerns about environmental sustainability and fossil fuel depletion, has accelerated the adoption of electric vehicles (EVs). Integrating renewable energy sources and advanced energy storage systems into EVs is viewed as a key strategy for improving efficiency, reducing emissions, and extending driving range. Among renewable options, photovoltaic (PV) arrays offer a clean and inexhaustible source of energy. However, their intermittent and weather-dependent nature necessitates coupling with reliable electrochemical storage units.

In this context, potassium-ion batteries (KIBs) have emerged as a promising alternative to lithium-ion batteries (LIBs), owing to their lower cost, environmental compatibility, abundance of potassium resources, and competitive electrochemical performance. In particular, KIBs

ISSN:2731-538X | E-ISSN:2731-5398
Vol. 20 No. 01 (2026)

employing $K_3V_2(PO_4)_3/C$ nanocomposite cathodes demonstrate high structural stability, long cycle life, and safety, making them suitable for transportation applications.

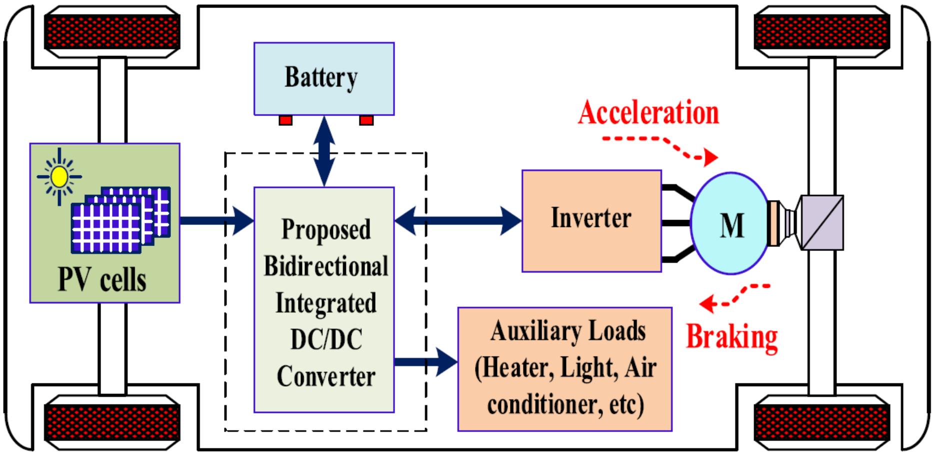

Fig 1 Proposed model block diagram

Efficient integration of PV arrays and KIBs into EVs requires a **multi-converter architecture** that manages power flow between renewable generation, battery storage, traction drives, and auxiliary loads as shown in fig1 and electrical circuit diagram in Fig 2 . Boost converters are used for PV arrays to enable maximum power point tracking (MPPT), bidirectional buck–boost converters regulate charging and discharging of the KIB, and auxiliary boost stages supply power to additional vehicle loads. To achieve reliable operation under variable irradiance, load fluctuations, and regenerative braking, these converters must be supported by closed-loop control strategies. Such strategies ensure stable DC-link voltage, optimal energy utilization, and extended battery life, thereby improving the overall reliability of EVs.

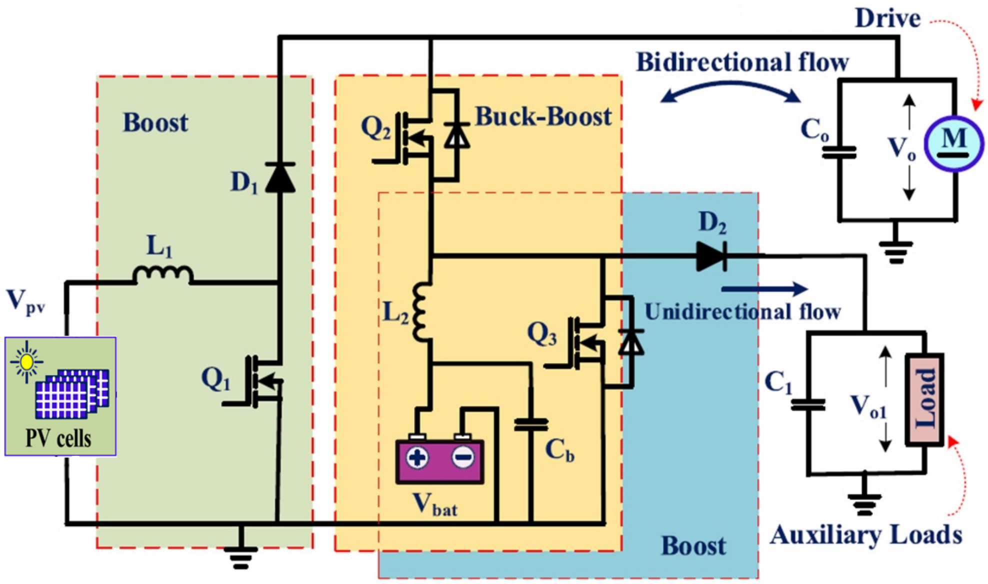

Fig 2 Proposed model circuit diagram

3.1 Modeling of $K_3V_2(PO_4)_3/C$ (PVP/C) Battery

ISSN:2731-538X | E-ISSN:2731-5398
Vol. 20 No. 01 (2026)

Accurate modeling of $K_3V_2(PO_4)_3/C$ (PVP/C) batteries is crucial for predicting their electrochemical and thermal behavior under various operating conditions in electric-vehicle (EV) applications. The PVP-assisted sol–gel-derived $K_3V_2(PO_4)_3/C$ nanocomposite exhibits a three-dimensional conductive carbon network that enhances electronic transport and provides stable potassium-ion diffusion channels. These properties yield a high discharge capacity of 122 mAh g^{-1}, a nominal voltage of 3.8 V, and outstanding cycling stability with 99 % capacity retention after 2000 cycles at 1000 mA g^{-1}. To replicate this performance in simulation, an integrated electrochemical–thermal–aging model was developed in MATLAB/Simulink.

The electrochemical behavior of the cell was described using an equivalent circuit representation based on the Thevenin approach. The model comprises an open-circuit voltage (OCV) source, an ohmic resistance R_0, and two RC polarization branches to account for charge-transfer and diffusion effects. The terminal voltage is given by

$$V_{term}=V_{oc}(SOC)-IR_0-V_1-V_2,$$

where V_1 and V_2 represent transient polarization voltages governed by the time constants R_1C_1 and R_2C_2. Parameter identification was performed using electrochemical impedance spectroscopy (EIS) data, where the charge-transfer resistance R_{ct} was approximately 101 Ω and the Warburg tail confirmed the diffusion-controlled process. The resulting parameter set (R_0=0.12Ω, R_1=0.18Ω, C_1=400F, R_2=0.32Ω, C_2=1500F) reproduced the experimental voltage response accurately.

State-of-charge (SOC) variation was computed by Coulomb counting using

$$SOC(t) = SOC_0 - \frac{1}{C_n}\int I(t)\,dt,$$

where Cn=0.122Ah. The OCV–SOC relationship was extracted from galvanostatic charge–discharge curves and expressed as a second-order polynomial. Thermal dynamics were incorporated through a lumped heat-balance model

$$C_{th}\frac{dT}{dt} = I^2R_0 + (V_{oc} - V_{term})I - \frac{T - T_{amb}}{R_{th}},$$

With C_{th}=900 $Jkg^{-1}K^{-1}$ and R_{th}=0.65°C $W^{-1}R_{th}$=0.65°CW^{-1}. The model predicted a modest temperature rise (< 8 °C) during 3C discharge, consistent with the high thermal stability (up to 350 °C) observed experimentally.

To capture long-term degradation, empirical aging laws were introduced for capacity fade and resistance growth:

$$Q_{loss}(N) = Q_0(1 - k_cN^{\alpha}), \qquad R(N) = R_0(1 + k_rN^{\beta}),$$

where $k_c=5\times10^{-5}$, $k_r=3\times10^{-5}$, and α=β=0.7. The simulated results mirrored experimental findings, showing only a 1 % capacity loss and 10 % resistance increase after 2000 cycles. The complete model was implemented in the Simscape *Battery* block with temperature and aging effects enabled, configured for a seven-cell (7S) pack providing 26.6 V and 0.854 Ah capacity.

Validation against laboratory data demonstrated excellent correlation between simulated and measured voltage, capacity, and temperature responses, with deviations below 2 %. The model therefore provides a reliable framework for system-level studies of potassium-ion batteries in EV applications. Its modular structure enables integration with energy storage systems and battery-

ISSN:2731-538X | E-ISSN:2731-5398
Vol. 20 No. 01 (2026)

management algorithms for real-time energy optimization. Overall, the developed $K_3V_2(PO_4)_3/C$ (PVP/C) model successfully bridges material-level electrochemical characteristics with pack-level dynamic behavior, enabling performance prediction, thermal assessment, and lifetime evaluation for next-generation safe and sustainable energy storage systems.

To address these challenges, various control strategies are implemented and evaluated for both voltage reference regulation and motor speed reference control. These include: Proportional-Integral Controller (PI), Fractional Order PID (FOPID), Sliding Mode Control (SMC), Model Predictive Control (MPC), Hysteresis Controller (HC), Fuzzy Logic Control (FLC)

The control of energy storage systems (ESS) integrated with photovoltaic (PV) generation and potassium-ion batteries demands precise regulation of DC-link voltage, current sharing, and state-of-charge (SOC) balancing to ensure stability and efficiency in electric vehicle (EV) applications. Various control techniques—both classical and advanced—are utilized to optimize system dynamics, reduce transients, and improve robustness under nonlinear and uncertain conditions.

3.2 Proportional–Integral (PI) controller

The Proportional–Integral (PI) controller remains the most widely implemented control method for voltage and current regulation in converter-based HESS architectures due to its structural simplicity and effectiveness in minimizing steady-state error. Recent studies have demonstrated that PI controllers, when properly tuned, can ensure DC-link voltage stability in renewable and vehicular energy systems. However, their performance degrades significantly under nonlinear operating conditions or parameter variations (Merai et al., 2019).

Principles of Operation

The proportional term provides a rapid response to changes in error by immediately adjusting the control output according to how far the system is from its desired setpoint. However, proportional-only control alone will typically leave a residual error (offset) since it always requires a nonzero error to actuate the system. The integral term addresses this limitation by summing the past errors; as long as there is any nonzero error, the integral action continues to increase, driving the control output to the point that the steady-state error is eliminated.

The classical continuous-time transfer function of the PI controller is

$$GPI(s)=Kp+Kis$$

where Kp is the proportional gain and Ki is the integral gain

The Proportional–Integral (PI) controller is one of the simplest and most widely used control strategies in power electronics and energy storage systems. It works by correcting the error between the reference and the actual output through two actions: the proportional term, which responds to the

ISSN:2731-538X | E-ISSN:2731-5398
Vol. 20 No. 01 (2026)

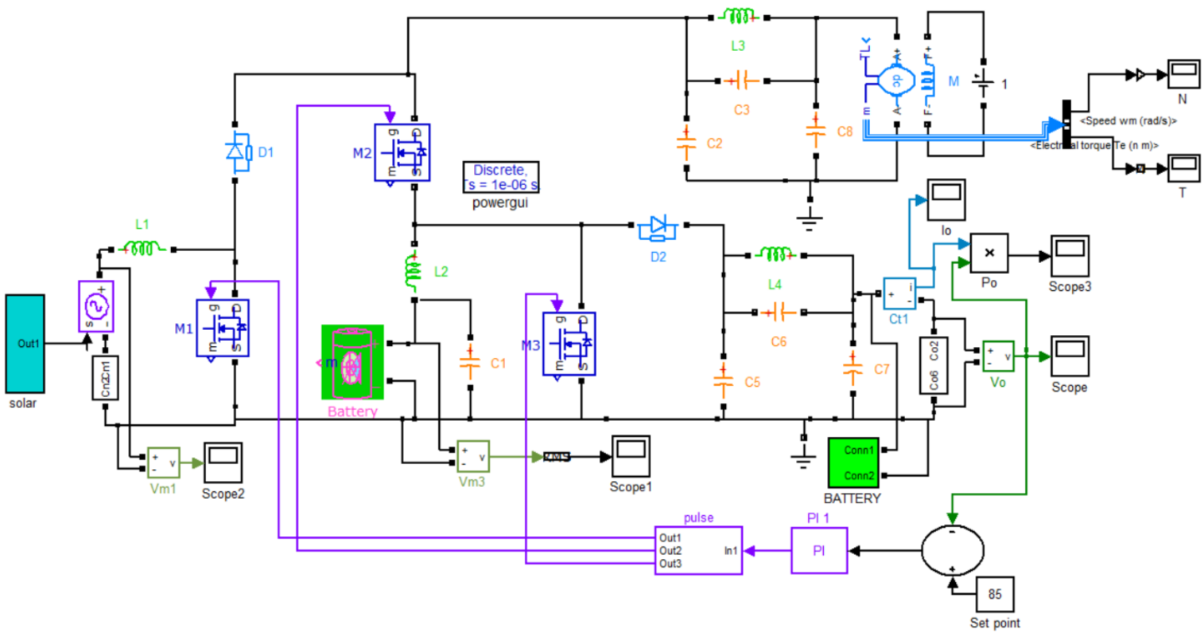

Fig. 3(a): Closed-loop block diagram of PI-controlled PV–KIB system

present error, and the integral term, which eliminates steady-state error by accumulating past deviations. In HESS applications, PI controllers are commonly used for DC-link voltage regulation, battery charging/discharging control, and motor speed regulation. Their major advantages include simple structure, easy implementation, and low computational requirements, making them suitable for real-time applications in PV–battery systems. However, PI controllers are less effective under nonlinear dynamics, rapidly changing operating conditions, or parameter uncertainties, which are inherent in renewable-integrated systems. Despite these limitations, they remain a baseline strategy for comparison with advanced control methods.

The Proportional–Integral (PI) controller serves as the baseline case in this study and is widely recognized for its simplicity and ease of implementation in power electronic systems. The closed-loop configuration of the PV–KIB system under PI control is shown in Fig. 3(a). The PI controller relies on two components: the proportional term, which provides immediate correction based on the magnitude of the error, and the integral term, which eliminates steady-state error by summing past deviations.

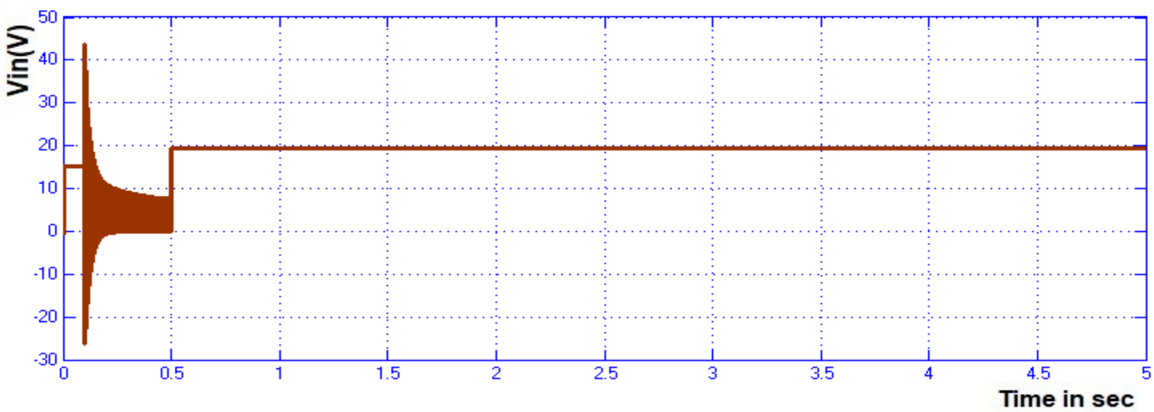

Fig. 3(b): PV array voltage response under PI controller

ISSN:2731-538X | E-ISSN:2731-5398
Vol. 20 No. 01 (2026)

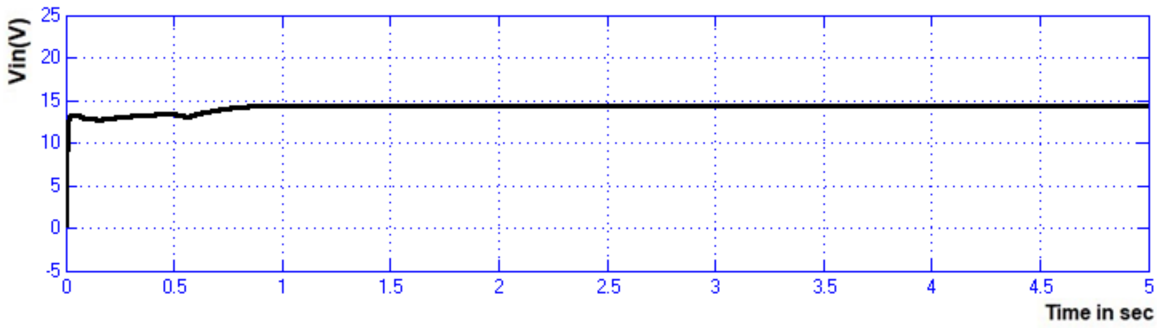

Fig. 9(c): Battery voltage regulation with PI-based bidirectional converter

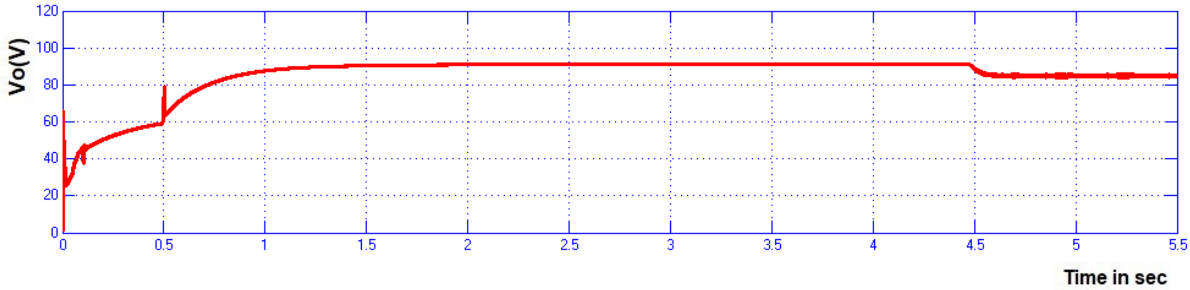

Fig. 3(d): DC bus/load voltage stabilization under PI control

The PV array voltage response in Fig. 9(b) demonstrates stabilization around 20 V. The time-domain analysis confirms a rise time of 0.8 s, a peak time of 1.2 s, and a settling time of 4.5 s, with a steady-state error of 2.79 V. These values highlight the sluggish nature of PI control, as the proportional action reacts quickly but the integral term accumulates slowly, causing delayed recovery under disturbances. Similarly, the battery voltage shown in Fig. 9(c) stabilizes near 15 V, but tracking is relatively slow, especially when the battery's state-of-charge (SOC) changes abruptly. This slow tracking again stems from the integral action, which eliminates error eventually but struggles with fast nonlinear variations.

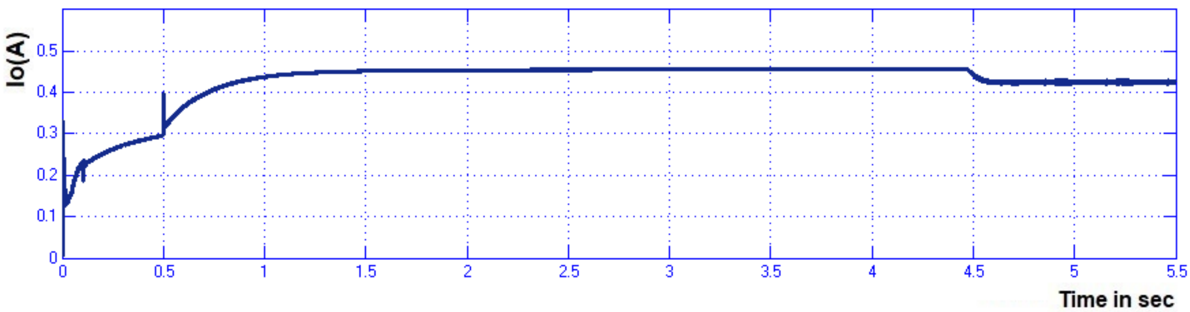

Fig. 3(e): Load current response with PI controller

ISSN:2731-538X | E-ISSN:2731-5398
Vol. 20 No. 01 (2026)

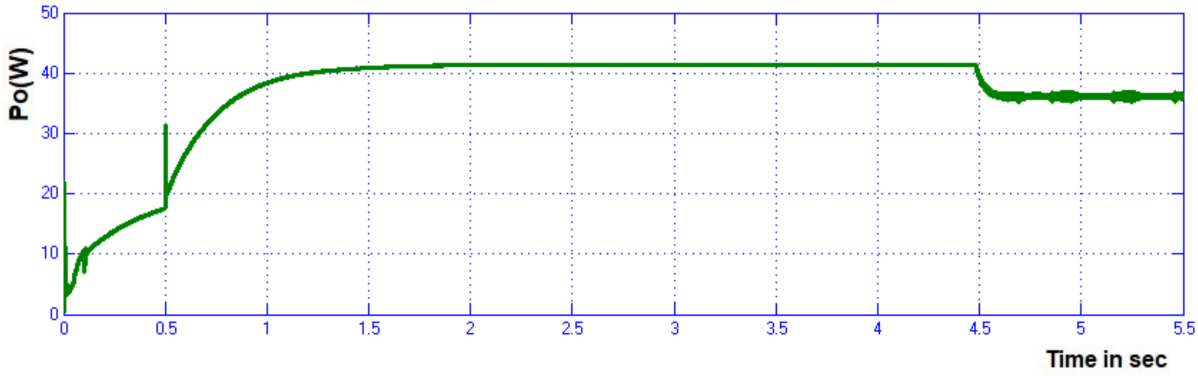

Fig. 3(f): Output power characteristics under PI control

The DC bus/load voltage regulation presented in Fig. 9(d) shows stabilization near 85 V. However, due to the linear structure of the PI controller, oscillations and ripples are evident, indicating poor handling of the switching nonlinearities in the bidirectional converter. This effect is more pronounced under source-side disturbances, such as solar irradiance fluctuations, where PI takes longer to restore stability. The load current and output power characteristics, shown in Figs. 9(e) and 9(f), stabilize at around 0.43 A and 36 W, respectively. These values are lower than expected because slower error correction leads to energy losses and reduces system efficiency.

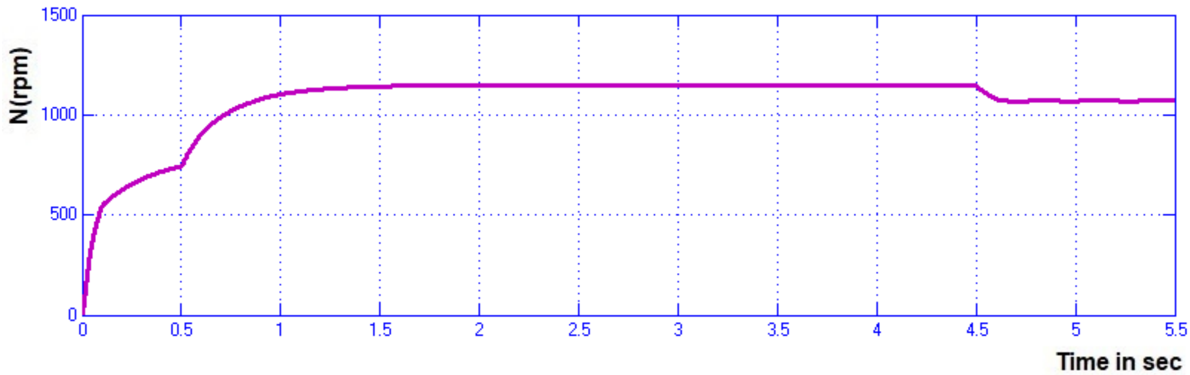

Fig. 3(g): Motor speed response with PI regulation

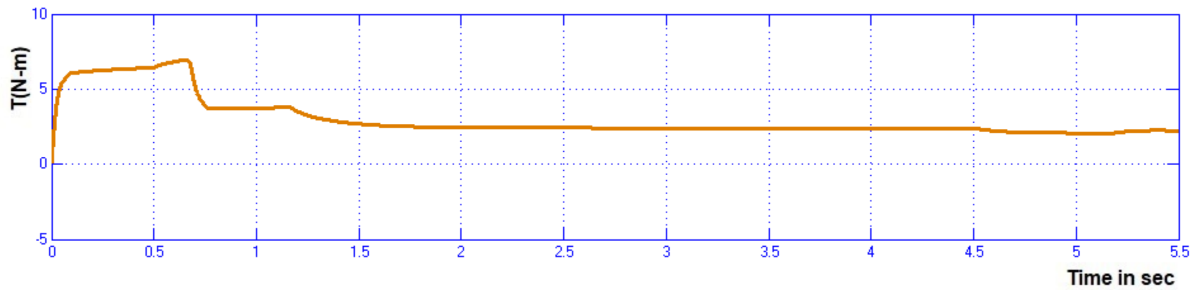

Fig. 3(h): Motor torque performance under PI controller

The motor speed and torque performance are illustrated in Figs. 9(g) and 9(h). The motor speed settles at approximately 1070 rpm and the torque at 2.2 N·m. Although steady-state values are achieved, the dynamic performance is weak. The time-domain parameters confirm a rise time of 0.7 s, a peak time of 1.1 s, a settling time of 4.61 s, and a steady-state error of 2.98 rpm. These results clearly show that the PI controller cannot meet the fast acceleration and precise tracking requirements of electric vehicle applications. The sluggish response and high steady-state error

ISSN:2731-538X | E-ISSN:2731-5398
Vol. 20 No. 01 (2026)

reduce both ride comfort and efficiency when deployed in real-time traction systems.

In summary, the PI controller provides a simple and computationally efficient solution for regulating PV voltage, battery charging, DC bus stability, and motor operation. However, its performance is characterized by long settling times, higher steady-state errors, and poor adaptability to nonlinearities and disturbances. While it ensures basic system stability, PI control falls short in meeting the stringent performance demands of PV–KIB systems in electric vehicle applications. It therefore serves primarily as a benchmark for evaluating the improvements achieved by advanced controllers.

3.3 FOPID Controller

The Fractional-Order PID (FOPID) controller, an extension of the traditional PID controller, introduces fractional calculus by allowing the integral and derivative orders to be non-integer. This provides enhanced flexibility for control tuning and improves robustness against model uncertainties. FOPID controllers have been reported to achieve superior transient response, improved disturbance rejection, and enhanced steady-state accuracy in hybrid energy and renewable systems (Podlubny, 1999; Monje et al., 2010; Alilou et al., 2023; Tepljakov et al., 2018).

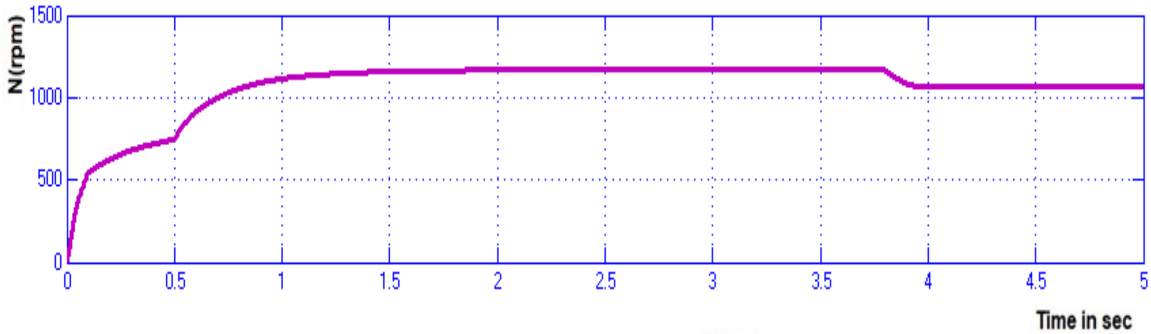

Fig. 4(a): Motor speed response with FOPID regulation

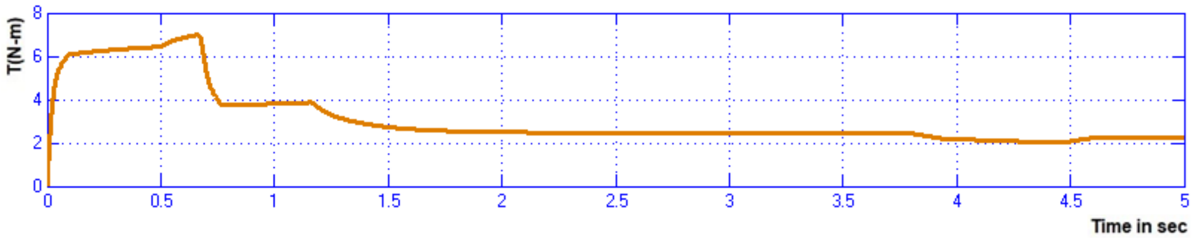

Fig. 4(b): Motor torque performance under FOPID controller

The motor performance, presented in Figs. 4(a) and 4(b), also reflects this improvement. The motor speed stabilizes at 1070 rpm and torque at 2.2 N·m, but with smoother tracking and fewer oscillations. The time-domain parameters for motor speed confirm a rise time of 0.6 s, a peak time of 0.85 s, a settling time of 4.2 s, and a steady-state error of 2.46 rpm. Compared to PI, the FOPID reduces rise time and error while providing smoother dynamics, though the settling time remains somewhat long due to the inherent system inertia.

3.4 Sliding Mode Control (SMC)

The Sliding Mode Control (SMC) technique offers a robust nonlinear control solution capable of handling system uncertainties and external disturbances by enforcing the system trajectory to follow a predefined sliding surface. This results in strong robustness and fast dynamic response,

ISSN:2731-538X | E-ISSN:2731-5398
Vol. 20 No. 01 (2026)

which makes SMC suitable for HESS and electric drive applications. However, its implementation often suffers from high-frequency chattering, leading to increased converter switching losses (Utkin, 1992; Slotine & Li, 1991; Darvish Falehi et al., 2021).

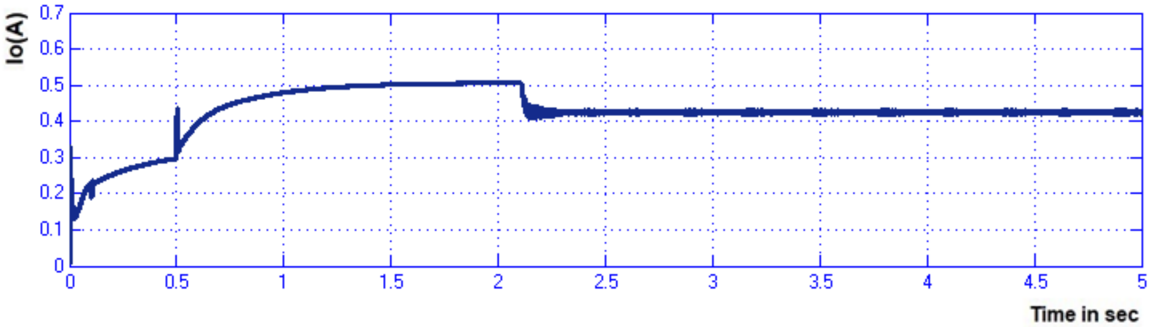

Fig. 5(a): Load current response with SMC controller

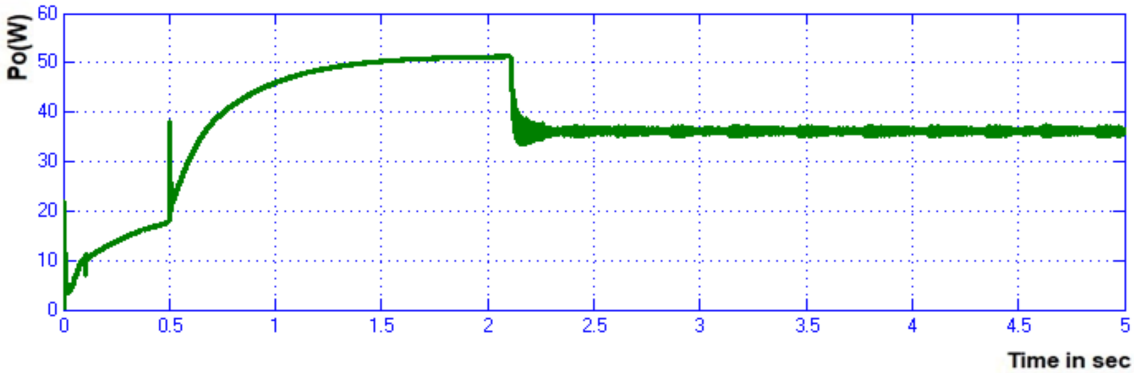

Fig. 5(b): Output power characteristics under SMC control

. The load current response in Fig. 5(a) remains near 0.43 A, while the output power shown in Fig. 5(b) reaches approximately 36 W. Both signals exhibit small oscillations that can be attributed to the chattering effect, a common drawback of sliding mode control where the high-frequency switching introduces ripple in the current and power waveforms.

3.5 Model Predictive Control (MPC)

Model Predictive Control (MPC), an optimization-based control strategy, predicts future system states and minimizes a cost function within defined constraints. Its ability to handle multiple variables and operational limits simultaneously has made it highly attractive for HESS and power converter systems. MPC ensures optimal current and voltage regulation while reducing stress on the energy sources. Despite these advantages, it requires significant computational resources and accurate system modelling (Camacho & Bordons, 2007; Bemporad et al., 2002; Arias et al., 2025).

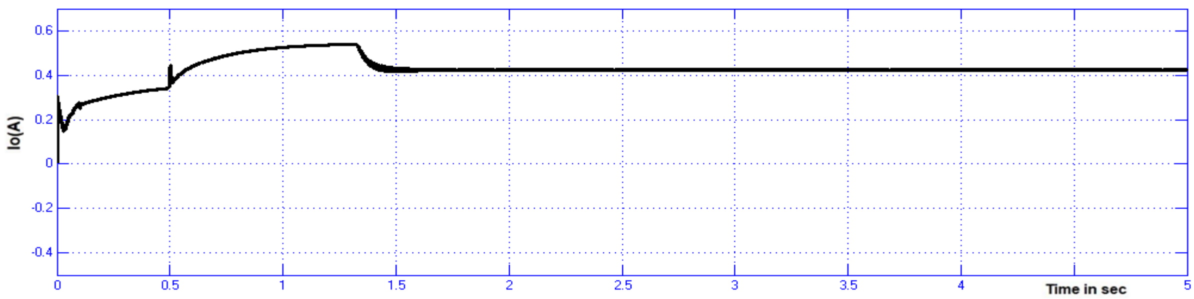

Fig. 6(a): Load current response with MPC controller

The load current and output power responses, shown in Figs. 19(e) and 19(f), remain highly stable

ISSN:2731-538X | E-ISSN:2731-5398
Vol. 20 No. 01 (2026)

at 0.43 A and 36 W. Time-domain analysis reveals smooth, ripple-free behavior with minimal transient oscillations. Compared to the oscillations observed in SMC and HC, MPC provides cleaner waveforms, which translates to lower switching losses and improved energy efficiency. This smoother current and power regulation also reduces stress on converter components and improves reliability in hardware implementation.

MPC delivers the best time-domain performance overall, with the fastest rise and settling times, lowest steady-state error, and smoothest dynamic behavior across PV voltage, battery regulation, DC bus stabilization, and motor performance. Its predictive ability ensures robustness against disturbances and high accuracy in real-time operation. However, its computational complexity and hardware cost limit its widespread deployment in low-cost EV systems. For high-performance applications where computational resources are available, MPC remains the most powerful control option.

3.6 Hysteresis Controller (HC)

Hysteresis Control (HC) is a simple nonlinear control technique that maintains the error within a defined hysteresis band, offering rapid transient response and strong disturbance rejection. Its main disadvantage lies in its variable switching frequency, which causes additional inverter losses and electromagnetic interference (Holmes & Lipo, 2003; Bose, 2002; Karthikkumar & Sheela, 2025).

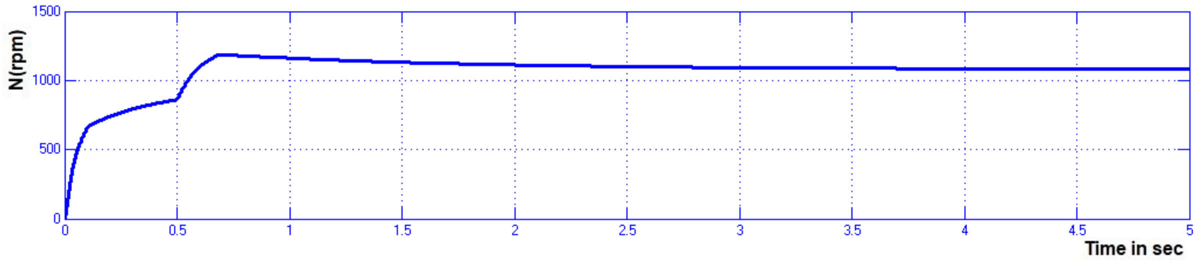

Fig. 7(g): Motor speed response with hysteresis regulation

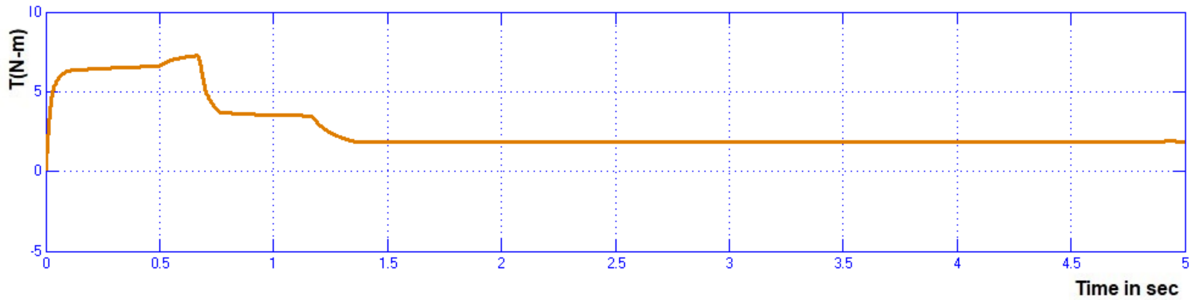

Fig. 7(h): Motor torque performance under hysteresis controller

Motor performance under hysteresis control is shown in Figs. 7(g) and 7(h). The motor speed reaches 1070 rpm and torque stabilizes at 2.2 N·m with one of the fastest transient responses among all controllers. The time-domain specifications for motor speed confirm a rise time of 0.25 s, a peak time of 0.42 s, a settling time of 1.46 s, and a steady-state error of 0.86 rpm. These values highlight HC's ability to deliver fast acceleration and stable operation, making it suitable for traction applications in electric vehicles where rapid torque response is critical. However, torque ripples caused by variable switching frequency may still appear, though they are generally less severe than the chattering observed in SMC.

3.7 Fuzzy Logic Controller (FLC)

ISSN:2731-538X | E-ISSN:2731-5398
Vol. 20 No. 01 (2026)

Fuzzy Logic Control (FLC) provides a model-free intelligent approach that applies linguistic rules and fuzzy inference for decision-making. This makes FLC highly suitable for nonlinear systems such as PV–battery-based hybrid converters. FLC can effectively handle uncertainties and parameter variations, though its accuracy heavily depends on expert-defined membership functions and rule bases (Zadeh, 1973; Mendel, 1995; Silva.A et al., 2024).

In the PV-potassium-ion battery energy storage system with bidirectional buck-boost converter examined in the chapter, fuzzy logic control offers superior time-domain performance compared to conventional PI and even fractional-order PID controllers. It delivers faster rise times, lower steady-state errors, and shorter settling times for both voltage and motor speed regulation tasks. This translates into enhanced system stability, efficiency, and adaptability under the complex, nonlinear operating conditions typical of electric vehicles

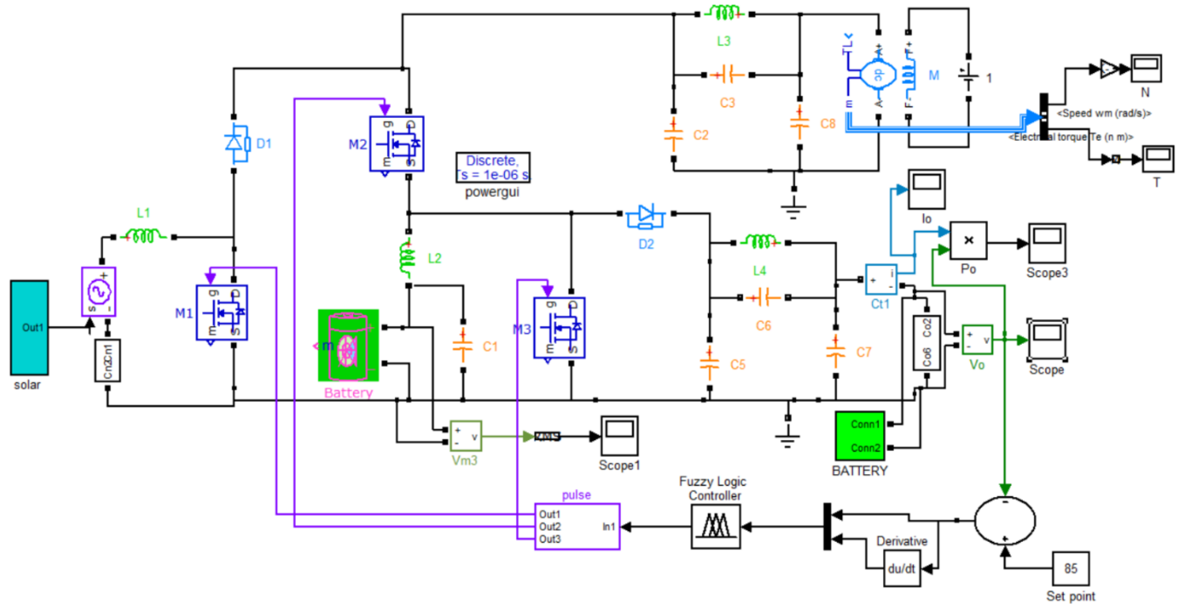

Fig. 8 (a): Closed-loop block diagram of FLC-controlled PV–KIB system

The Fuzzy Logic Controller (FLC) is a knowledge-based, nonlinear control method that uses linguistic rules and membership functions instead of a precise mathematical model. This makes FLC particularly suitable for systems with uncertainties, nonlinearities, and variable operating conditions, such as hybrid PV–KIB systems. The closed-loop configuration under FLC regulation is shown in Fig. 8(a). The ability of FLC to adapt dynamically allows it to maintain stable operation under fluctuating PV input and varying battery SOC, while offering smooth power delivery and reliable motor control.

ISSN:2731-538X | E-ISSN:2731-5398
Vol. 20 No. 01 (2026)

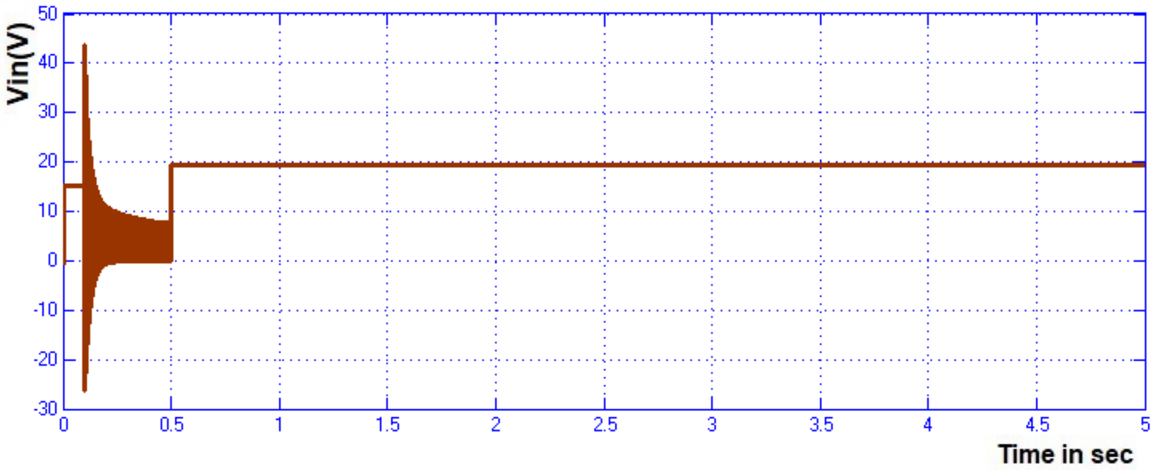

Fig. 8(b): PV array voltage response under fuzzy logic controller

The PV array voltage response in Fig. 8(b) demonstrates precise regulation at 20 V. Time-domain analysis confirms a rise time of 0.2 s, a peak time of 0.35 s, a settling time of 0.83 s, and a steady-state error of only 0.66 V. These values represent the fastest and most accurate PV voltage regulation among all controllers. Unlike PI and FOPID, which rely on fixed gains, or SMC and HC, which suffer from oscillations, the FLC adapts its control action in real time through fuzzy inference, ensuring smooth and rapid stabilization.

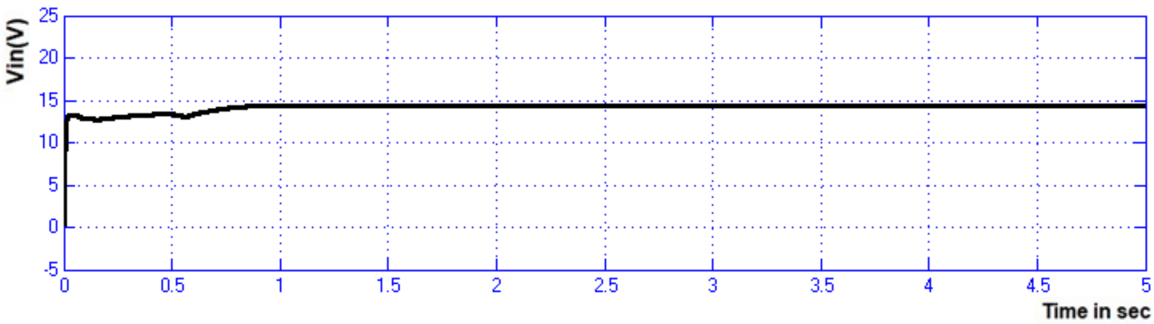

Fig. 8(c): Battery voltage regulation with fuzzy logic controller

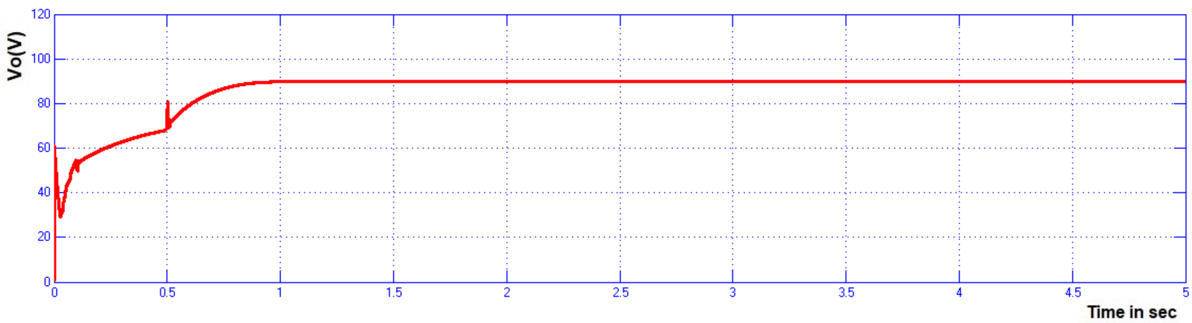

Fig. 8(d): DC bus/load voltage stabilization under fuzzy logic control

The battery voltage regulation shown in Fig. 8(c) stabilizes effectively at 15 V, even under dynamic SOC variations. The fuzzy inference system ensures fast correction by interpreting deviations through fuzzy rules, allowing smoother transitions than PI or HC and avoiding oscillations typical of SMC. The DC bus/load voltage response in Fig. 8(d) further demonstrates the superiority of FLC. The bus voltage stabilizes at 85 V with the shortest settling time of 0.83 s and the lowest steady-state error of 0.66 V. This ensures reliable DC bus operation, which is critical for powering vehicle motors and auxiliary loads.

ISSN:2731-538X | E-ISSN:2731-5398
Vol. 20 No. 01 (2026)

The load current and output power responses, illustrated in Figs. 8(e) and 8(f), remain stable at approximately 0.43 A and 36 W, with minimal ripple. Time-domain specifications indicate very fast rise and peak times, with smooth settling, outperforming PI and HC, which showed either sluggish behavior or oscillations. This confirms FLC's effectiveness in minimizing energy losses and maintaining consistent power delivery.

Motor dynamics highlight the strongest improvements under FLC. The motor speed response in Fig. 8(g) reaches 1070 rpm rapidly and with high precision, while torque in Fig. 8(h) stabilizes smoothly at 2.2 N·m. Time-domain specifications for motor speed confirm a rise time of 0.2 s, a peak time of 0.34 s, a settling time of 1.12 s, and a steady-state error of just 0.96 rpm. These values make FLC the best-performing controller for motor drive operation, offering both fast acceleration and smooth torque transfer—crucial features for electric vehicle traction applications.

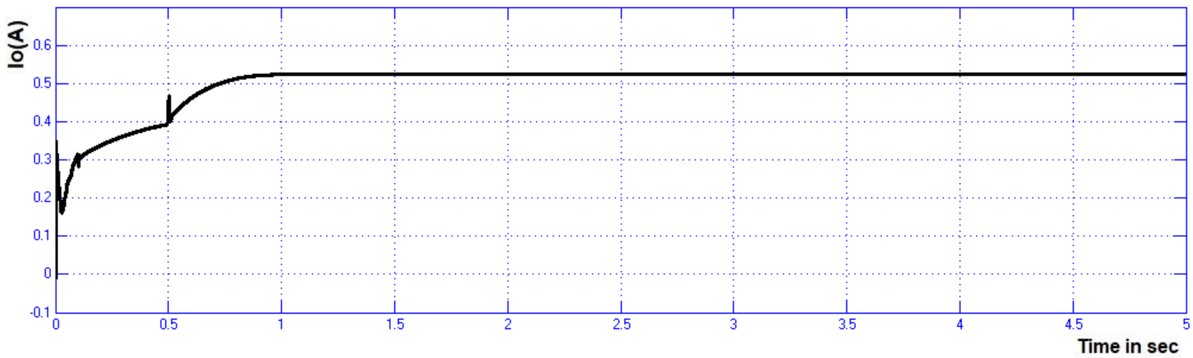

Fig. 8(e): Load current response with fuzzy logic controller

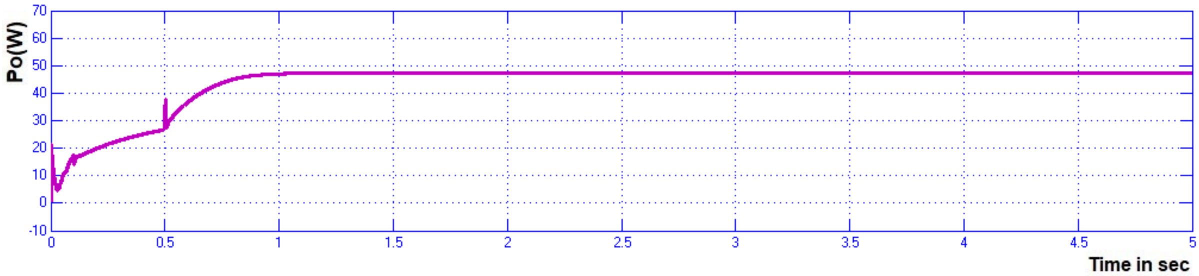

Fig. 8(f): Output power characteristics under fuzzy logic control

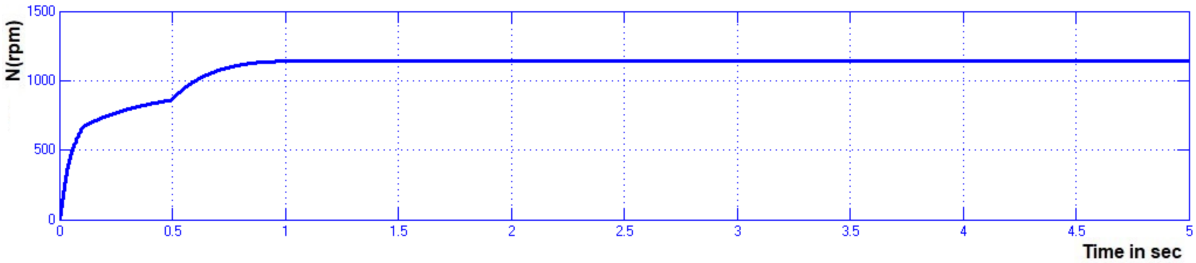

Fig. 21(g): Motor speed response with fuzzy regulation

ISSN:2731-538X | E-ISSN:2731-5398
Vol. 20 No. 01 (2026)

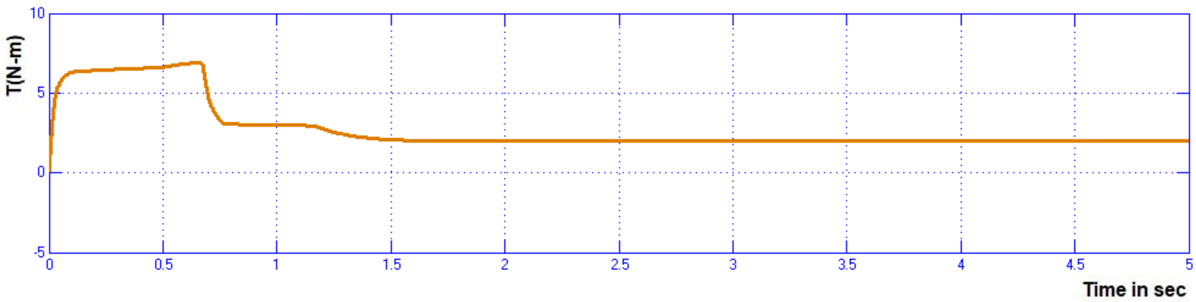

Fig. 8(h): Motor torque performance under fuzzy logic controller

From a hardware perspective, FLC is practical and less computationally demanding than MPC or FOPID. It can be implemented on moderate-capacity microcontrollers or DSPs with fuzzy inference capability. However, the main limitation of FLC lies in the design of its rule base and membership functions, which requires expert knowledge and may lack guaranteed mathematical optimality. Nevertheless, once properly designed, FLC achieves an excellent balance of accuracy, speed, and robustness.

The Fuzzy Logic Controller demonstrates the best overall performance across all tested parameters. It achieves the fastest rise and settling times, lowest steady-state error, smooth power flow, and superior motor dynamics, all while being computationally feasible for hardware implementation. These qualities make FLC the most practical and effective control strategy for PV–KIB systems in electric vehicles.

3.8. Comparison of Time-Domain Parameters for Voltage Reference

The time-domain specifications of different controllers for voltage regulation are summarized in Table-1. The PI controller exhibits the slowest response, with a rise time of 0.8 s, a peak time of 1.2 s, and a settling time of 4.5 s, along with the highest steady-state error of 2.79 V. This confirms its limited suitability for handling fast disturbances. The FOPID controller improves performance with a reduced rise time (0.6 s) and settling time (3.8 s), and a lower error (2.34 V) compared to PI.

Table-1. Comparsion Time Domain Parameters for voltage reference

Controllers	Rise time (s)	Peak time (s)	Setting time (s)	Steady state error (V)
PI	0.8	1.2	4.5	2.79
FOPID	0.6	0.95	3.8	2.34
SMC	0.54	1.85	2.14	1.42
MPC	0.52	1.30	1.50	0.95
HC	0.51	0.69	1.14	0.86
FLC	0.50	0.62	0.83	0.66

The nonlinear controllers demonstrate significantly better performance. Sliding Mode Control (SMC) reduces the settling time to 2.14 s and error to 1.42 V, though its peak time (1.85 s) is longer than FOPID and MPC due to chattering effects. Model Predictive Control (MPC) achieves superior accuracy, with the fastest response among advanced controllers (rise time 0.52 s, settling time 1.5 s, error 0.95 V). The Hysteresis Controller (HC) further reduces settling time to 1.14 s, though variable switching causes minor fluctuations. The Fuzzy Logic Controller (FLC) achieves the best performance overall, with a rise time of 0.50 s, settling time of 0.83 s, and the lowest error of 0.66 V.

The comparison is clearly visualized in Fig. 9, where FLC consistently outperforms all other controllers across all parameters. This confirms that fuzzy rule-based adaptation ensures rapid and accurate voltage regulation under source disturbances.

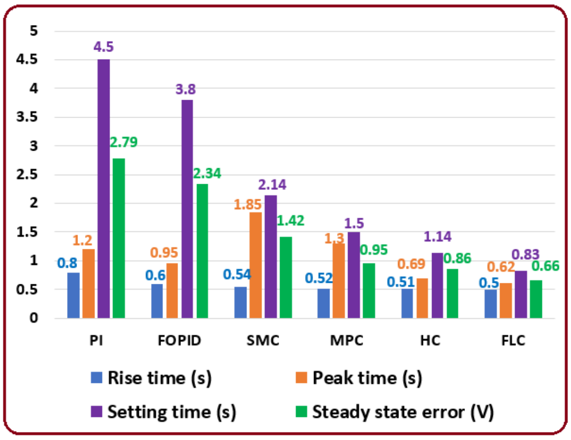

Fig-9. Bar graph Comparsion of Time Domain Parameters for voltage reference

3.9 Comparison of Time-Domain Parameters for Motor Speed Reference

The time-domain results for motor speed control are presented in Table-2. The PI controller again shows the weakest performance, with a rise time of 0.7 s, settling time of 4.61 s, and a steady-state error of 2.98 rpm. The FOPID controller improves upon PI, reducing rise time to 0.6 s and error to 2.46 rpm, though its settling time (4.2 s) remains high due to the complexity of motor dynamics.

Among advanced controllers, SMC stabilizes the motor in 2.45 s with an error of 1.50 rpm, demonstrating robust performance but with minor oscillations. MPC achieves faster stabilization, with a rise time of 0.54 s, a settling time of 1.7 s, and reduced error of 1.10 rpm, showing the predictive controller's ability to handle dynamic load changes effectively. HC further improves transient performance, achieving a settling time of 1.46 s and an error of 1.14 rpm, reflecting its ability to enforce tight error bounds. The best performance is achieved by the FLC, which exhibits the shortest rise time (0.51 s), fastest settling time (1.12 s), and lowest error (0.96 rpm), resulting in smooth and accurate speed regulation.

The results are summarized in the table 2 for motor speed reference, where it is evident that FLC outperforms all other controllers, closely followed by HC and MPC. These findings confirm that FLC provides the best balance between speed of response, accuracy, and robustness for motor drive applications in PV–battery systems.

Table-2. Comparsion of Time Domain Parameters for motor speed reference

Controllers	Rise time (s)	Peak time (s)	Setting time (s)	Steady state error (rpm)
PI	0.7	1.1	4.61	2.98
FOPID	0.6	0.85	4.2	2.46
SMC	0.57	1.00	2.45	1.50
MPC	0.54	0.85	1.70	1.10
HC	0.53	0.71	1.46	1.14

ISSN:2731-538X | E-ISSN:2731-5398
Vol. 20 No. 01 (2026)

FLC	**0.51**	**0.69**	**1.12**	**0.96**

4. **Conclusion and Future Work**

This study presented the design, modeling, and evaluation of a photovoltaic powered potassium-ion batteries (KIBs) $K_3V_2(PO_4)_3/C$ Nano composites for electric vehicle (EV) applications. Six control strategies—PI, FOPID, SMC, MPC, HC, and FLC—were systematically implemented and compared in terms of voltage regulation, power management, and motor performance. Simulation and experimental results confirmed that KIB-based ESS can effectively stabilize DC-link voltage, support regenerative braking, and provide smooth traction operation under fluctuating irradiance and load conditions. While conventional PI offered simplicity, its performance degraded under nonlinear dynamics. FOPID improved tracking accuracy, and SMC provided robustness but suffered from chattering. HC achieved fast response but variable switching frequency limited efficiency. FLC offered adaptability and robustness without requiring detailed system models, while MPC consistently delivered the best overall performance with the lowest errors, fastest dynamics, and precise motor control. The findings establish the feasibility of integrating KIBs into renewable-assisted EVs, highlighting their potential as sustainable alternatives to lithium-ion batteries. Moreover, the comparative control analysis provides valuable insights into selecting suitable EMS strategies for high-efficiency HESS.

5. References

[1] International Energy Agency (IEA), *CO2 Emissions from Fuel Combustion 2022*, IEA, Paris, 2022.

[2] Nitta, N., Wu, F., Lee, J. T., Yushin, G., Li-ion battery materials: Present and future, *Materials Today*, 18(5) (2015) 252–264. https://doi.org/10.1016/j.mattod.2014.10.040

[3] Goodenough, J. B., Park, K. S., The Li-ion rechargeable battery: A perspective, *Journal of the American Chemical Society*, 135(4) (2013) 1167–1176. https://doi.org/10.1021/ja3091438

[4] Zubi, G., Dufo-López, R., Carvalho, M., Pasaoglu, G., The lithium-ion battery: State of the art and future perspectives, *Renewable and Sustainable Energy Reviews*, 89 (2018) 292–308. https://doi.org/10.1016/j.rser.2018.03.002

[5] Olivetti, E. A., Ceder, G., Gaustad, G. G., Fu, X., Lithium-ion battery supply chain considerations: Analysis of potential bottlenecks in critical metals, *Joule*, 1(2) (2017) 229–243. https://doi.org/10.1016/j.joule.2017.08.019

[6] Wang, Q., Ping, P., Zhao, X., Chu, G., Sun, J., Chen, C., Thermal runaway caused fire and explosion of lithium ion battery, *Journal of Power Sources*, 208 (2012) 210–224. https://doi.org/10.1016/j.jpowsour.2012.02.038

[7] Eftekhari, A., Potassium secondary cell based on Prussian blue cathode, *Journal of Power Sources*, 343 (2017) 395–399. https://doi.org/10.1016/j.jpowsour.2017.01.073

[8] Komaba, S., Hasegawa, T., Dahbi, M., Kubota, K., Potassium intercalation into graphite to realize high-voltage/high-power potassium-ion batteries, *Electrochemistry Communications*, 60 (2015) 172–175. https://doi.org/10.1016/j.elecom.2015.08.018

[9] Okoshi, M., Yamada, Y., Yamada, A., Nakai, H., Theoretical analysis of interactions between potassium ions and organic electrolyte solvents: A comparison with lithium, sodium, and magnesium ions, *Journal of The Electrochemical Society*, 163(2) (2016) A54–A63.

https://doi.org/10.1149/2.0231602jes
[10] Sun, Y., Guo, S., Zhou, H., Adverse effects of trace water on the electrochemical performance of K-ion batteries, *Energy & Environmental Science*, 10 (2017) 1110–1116. https://doi.org/10.1039/C6EE03729G
[11] Kubota, K., Wang, Y., Komaba, S., Potassium-ion batteries—New frontiers in energy storage, *Advanced Energy Materials*, 8(16) (2018) 1703415. https://doi.org/10.1002/aenm.201703415
[12] Kim, H., et al., New K-ion battery cathode material: $K_3V_2(PO_4)_3$ with NASICON-type structure, *Advanced Energy Materials*, 6(18) (2016) 1600943. https://doi.org/10.1002/aenm.201600943
[13] Xiang, X., Zhang, K., Chen, J., Recent advances and prospects of cathode materials for K-ion batteries, *Advanced Materials*, 30(43) (2018) 1704633. https://doi.org/10.1002/adma.201704633
[14] Ehsani, M., Gao, Y., Gay, S. E., Emadi, A., *Modern Electric, Hybrid Electric, and Fuel Cell Vehicles: Fundamentals, Theory, and Design*, CRC Press, Boca Raton, 2018.
[15] Rahman, S., et al., Hybrid energy storage system for hybrid electric vehicles: A review, *Journal of Energy Storage*, 32 (2020) 101856. https://doi.org/10.1016/j.est.2020.101856
[16] Podlubny, I., Fractional-order systems and PIλDμ-controllers, *IEEE Transactions on Automatic Control*, 44(1) (1999) 208–214. https://doi.org/10.1109/9.739144
[17] Utkin, V. I., Sliding mode control design principles and applications to electric drives, *IEEE Transactions on Industrial Electronics*, 40(1) (1993) 23–36. https://doi.org/10.1109/41.184818
[18] Qin, S. J., Badgwell, T. A., A survey of industrial model predictive control technology, *Control Engineering Practice*, 11(7) (2003) 733–764. https://doi.org/10.1016/S0967-0661(02)00186-7
[19] Zadeh, L. A., Fuzzy logic, neural networks, and soft computing, *Communications of the ACM*, 37(3) (1994) 77–85. https://doi.org/10.1145/175247.175255
[20] Bose, B. K., Artificial intelligence techniques in smart grid and renewable energy systems—Some example applications, *Proceedings of the IEEE*, 105(11) (2017) 2262–2273. https://doi.org/10.1109/JPROC.2017.2757320
[21] Merai, M., Naouar, M.W., Slama-Belkhodja, I., & Monmasson, E. (2019). An Adaptive PI Controller Design for DC-Link Voltage Control of Single-Phase Grid-Connected Converters. *IEEE Transactions on Industrial Electronics, 66*, 6241-6249.
[22] Podlubny, I. (1999). Fractional-order systems and fractional-order controllers. *IEEE Transactions on Automatic Control, 44*(1), 208–213. https://doi.org/10.1109/9.739144
[23] Monje, C. A., Chen, Y., Vinagre, B. M., Xue, D., & Feliu, V. (2010). *Fractional-order Systems and Controls: Fundamentals and Applications.* Springer.
[24] Alilou, M., Azami, H., Oshnoei, A., Mohammadi-Ivatloo, B., & Teodorescu, R. (2023). Fractional-Order Control Techniques for Renewable Energy and Energy-Storage-Integrated Power Systems: A Review. *Fractal and Fractional, 7*(5), 391. https://doi.org/10.3390/fractalfract7050391
[25] Tepljakov, A., Petlenkov, E., & Belikov, J. (2018). Fractional-order PID control of a DC motor using model reduction and frequency domain design. *IFAC-PapersOnLine, 51*(4), 633–638. https://doi.org/10.1016/j.ifacol.2018.06.166

ISSN:2731-538X | E-ISSN:2731-5398
Vol. 20 No. 01 (2026)

[26] Utkin, V. I. (1992). *Sliding Modes in Control and Optimization.* Springer-Verlag.
[27] Slotine, J.-J. E., & Li, W. (1991). *Applied Nonlinear Control.* Prentice Hall.
[28] Darvish Falehi, A., Kaboli, S. H. A., & Gharehpetian, G. B. (2021). Robust fractional-order super-twisting sliding mode control to accurately regulate lithium-battery/super-capacitor hybrid energy storage systems. *International Journal of Energy Research, 45*(9), 13031–13048. https://doi.org/10.1002/er.7045
[29] Camacho, E. F., & Bordons, C. (2007). *Model Predictive Control (2nd ed.).* Springer.
[30] Bemporad, A., Morari, M., Dua, V., & Pistikopoulos, E. N. (2002). The explicit linear quadratic regulator for constrained systems. *Automatica, 38*(1), 3–20. https://doi.org/10.1016/S0005-1098(01)00174-1
[31] Arias, P., Farrés, M., Clemente, A., & Trilla, L. (2025). Model Predictive Control of a Hybrid Li-Ion Energy Storage System with Integrated Converter Loss Modeling. *Energies, 18*(20), 5462. https://doi.org/10.3390/en18205462
[32] Holmes, D. G., & Lipo, T. A. (2003). *Pulse Width Modulation for Power Converters: Principles and Practice.* IEEE Press.
[33] Bose, B. K. (2002). *Modern Power Electronics and AC Drives.* Prentice Hall.
[32] Karthikkumar, S., & Sheela, A. (2025). Implementation of adaptive hysteresis current controller in grid-tied multilevel converter with battery storage system. *Scientific Reports, 15*, 2974. https://doi.org/10.1038/s41598-025-02974-0
[33] Zadeh, L. A. (1973). Outline of a new approach to the analysis of complex systems and decision processes. *IEEE Transactions on Systems, Man, and Cybernetics, 3*(1), 28–44. https://doi.org/10.1109/TSMC.1973.5408575
[32] Mendel, J. M. (1995). Fuzzy logic systems for engineering: A tutorial. *Proceedings of the IEEE, 83*(3), 345–377. https://doi.org/10.1109/5.364485
[33] Silva, A., Amaro, M., & Mirez, J. (2025). Design of a Fuzzy Logic Control System for a Battery Energy Storage System in a Photovoltaic Power Plant to Enhance Frequency Stability. *Energies*, *18*(17), 4550. https://doi.org/10.3390/en18174550.